JOURNAL OF PROPULSION AND POWER
Vol. 11, No. 1, January–February 1995

Use of Swirl-Induced Particle Separation to Clean Nuclear Rocket Plumes

D. Oh* and D. Hastings†
Massachusetts Institute of Technology, Cambridge, Massachusetts 02139

A detailed computational analysis is undertaken of a vortex cleaning system designed to remove radioactive particulates from the plumes of nuclear rockets. An axisymmetric, inviscid flow model coupled with particle-tracking is used to analyze swirling flow in a nuclear rocket. The model shows that under some conditions a vortex-based particle removal system can have removal efficiencies of over 99%. However, it is also shown that the effectiveness of the system depends heavily on the size and density of the particles in the flow. Two critical parameters, the particle coupling velocity and a dimensionless frequency, are shown to govern the effectiveness of the system. These parameters are based on the length of the separation chamber, the swirl velocity, and the composition of particulates in the plume. It is concluded that the system can have negligible specific impulse losses associated with it, although there may be very substantial mass and thrust penalties associated with its use.

Nomenclature

a = radius of particulate
C_d = drag coefficient
C_p = specific heat at constant pressure
C_v = specific heat at constant volume
c = local speed of sound
D = damping vector
E, F = flux vectors
F_c = centrifugal force on particulate
F_d = magnitude of drag force on particulate
$F_{dr}, F_{dz}, F_{d\theta}$ = components of drag on particulate
F_{pr} = radial pressure force on particulate
G = source vector
H_∞ = total enthalpy
I_{sp} = specific impulse
J_- = Riemann invariant
M = molecular weight
m = mass of particulate
P_c = chamber pressure
p = local pressure
Re = Reynolds number
R_s = distance from centerline to skimmer
R_0 = radius of separation chamber
r = radial position
s = entropy
s_r = skimming ratio
T = temperature
T_c = chamber temperature
t_s = separation time
U = fluid state vector
$u_{p\theta}$ = particle tangential velocity
u_r = flow radial velocity
u_z = flow axial velocity
u_θ = flow tangential velocity
V = fluid velocity vector
V_p = particle velocity vector
v_c = critical coupling velocity
z = axial position
γ = ratio of specific heats
η = cleaning efficiency
η' = radius based cleaning efficiency
η'_0 = radius based efficiency when $s_r = 0$
θ = angular position
μ = viscosity
ν = dimensionless frequency
ρ = density of fluid
ρ_c = chamber density
ρ_p = density of particle
ψ = flow turning angle
Ω = vorticity vector
Ω_z = axial component of vorticity
$\overline{\Omega}^{(2,2)}$ = average effective collision integral
ω = fluid rotation rate

Received April 26, 1993; revision received March 16, 1994; accepted for publication May 19, 1994.

*Research Assistant.
†Professor of Aeronautics and Astronautics. Associate Fellow AIAA.

Introduction

NUCLEAR thermal rockets have existed as a concept since the 1950s, and offer a combination of high thrust and high specific impulse that make them ideal systems for the transportation of large payloads in a timely manner. Over the past two decades, a great deal of experimental and theoretical work has been done on these systems and, given the need, solid-core rockets could be built and flown within the decade. However, the presence of radioactive material creates very serious safety and contamination issues if these devices are to be ground-tested or used in the near-Earth environment. In particular, during the NERVA tests of the 1960s, it was observed that solid-core rockets can emit highly radioactive hydrogen plumes. These plumes not only make these systems difficult and expensive to test, but may contaminate the area on and around the spacecraft with radioactive material. At present, there is little experimental data available on the composition of these plumes, but judging from what is available, it is reasonable to assume that both gaseous and solid radioactive material will be present in the exhaust plume.[1] This article describes a system that would use artificially induced swirl to remove solid material from the exhaust plume before it leaves the rocket nozzle. It outlines the proposed system, describes the computational model used to analyze it, and discusses the parameters that govern its overall effectiveness. This article includes a detailed description of the system, a list of significant system parameters, charts showing its theoretical effectiveness, and a brief discussion of the penalties associated with its use.

Background

The basic principle behind swirl-based particle separation is simple: since the radioactive material in the plume has a much higher density than hydrogen gas, centrifugal forces can be used to force it to the outside of the flow where it can be "skimmed" off before it passes through the nozzle. Such forces can be created by passing the flow through a fixed vane swirler and creating a vortex in a separation chamber. A diagram of the proposed system is shown in Fig. 1.

Centrifugal separation systems have been used for decades in chemical processing and uranium enrichment systems. The proposed system is similar to these ground-based systems, but because it is intended that the system be usable in flight, it must be able to separate the material relatively quickly. Under typical conditions, the hydrogen propellant might leave the combustion chamber at velocities near 1100 m/s (Mach number = 0.3). Therefore, if the separation chamber is a meter in length, the separation time must be on the order of a millisecond.

Once the flow has passed through the separation chamber, its outer portion can be skimmed off and filtered to remove the radioactive material. The nonradioactive portion of the flow can then be returned to the reactor and reused as a propellant. The result is a regenerative cleaning scenario that limits the engine's I_{sp} losses (although the lost mass flow still lowers the thrust of the system). There are additional performance penalties associated with the mass of the separation chamber, the filtering system, and their associated cooling systems, but this article does not examine these issues. Rather, it deals with the vortex separation process and the ability of this system to keep radioactive material from escaping out the rocket nozzle. The specifics of the filtering and cooling process are left for future work. (Information on one filtering system designed for use on the ground is available in Ref. 1, but the system discussed is not directly applicable to this work.)

While vortex separation can theoretically be used with both solid and gaseous radioactive material, this article consists of a computational and analytical study of a particle removal system. For this study, it is assumed that the system is coupled to a NERVA class nuclear rocket with a nominal thrust of 300,000 N, a nominal chamber pressure of 29 atm, and a chamber temperature of 2500 K. The system has a throat radius of 0.119 m, a chamber radius of 0.148 m, and is assumed to be operating in vacuum. This results in an axial velocity of approximately 1100 m/s (Mach number = 0.3) in the separation chamber.

Although the propellant should not come into direct contact with the radioactive portions of solid-core nuclear reactors, ground-based furnace experiments indicate that nuclear rocket plumes can carry substantial amounts of radioactivity that may include solid radioactive material.[1] Any solid material present is likely to consist of eroded moderator mixed with metallic fission products that left the core in gaseous form and condensed after reaching the flow. To date, no experimental data is available about the size or distribution of particles in the plume. Therefore, several assumptions are made about the composition of the material in the plume. Any solid material present is assumed to consist of solid, spherical particles distributed uniformly across the flow. These particles are assumed to be composed of solid graphite or uranium with diameters ranging from 2 to 200 μm; an arbitrarily chosen range of distributions that corresponds roughly to the distribution of aluminum oxide particles in a solid rocket booster.[2] It is also assumed that any particle that reaches the outer wall of the channel will remain in the boundary layer and will not rebound off the wall back into the center of the flow. This implies that any particle that can be caught by a skimmer placed at a given position in the channel can also be caught by a skimmer placed downstream of that position. The implications of this assumption are discussed in the section on particle-wall interaction effects.

The effectiveness of the cleaning system can be expressed in terms of two figures of merit. The overall cleaning efficiency of the system η is defined to be

$$\eta = (n_p/N_p) \tag{1}$$

where n_p is the number of particles removed from the flow, and N_p is the total number of particles initially present in the flow. This parameter represents the fraction of the radioactive material removed from the flow. It is also convenient to define a radius based cleaning efficiency as follows

$$\eta' = [(R_0 - R_\eta)/R_0] \tag{2}$$

where R_η is the initial radial location of the innermost particle that is removed from the flow. All particles that enter the channel with an initial radial location greater than or equal to R_η are skimmed off, and all particles with an initial radial location less than R_η continue out the end of the nozzle. If the particles enter the channel with a uniform distribution, η and η' are related as follows:

$$\eta = 1 - (1 - \eta')^2 \tag{3}$$

Finally, a useful system design parameter is the skimming ratio s_r, which represents the portion of the total flow radius removed by the particle skimmer. It is defined as

$$s_r = [(R_0 - R_s)/R_0] \tag{4}$$

The skimming ratio is a design parameter, not a measure of efficiency, and specifies the width of the skimmer. It is related, but not identical to, the fraction of the total mass flow removed by the skimmer.

Computational Model

In order to study the swirl separation process, a two-part computational simulation has been developed to model the motion of particles in a swirling flow. The first part consists of an inviscid flow solver to model the hydrogen in the channel, and the second of a particle tracker to model the motion of particles in the flow. The simulation was run on a 189 × 70 Cartesian grid that simulates a constant radius channel with a choked exit. The choked exit simplified the boundary conditions by making the flow supersonic at the exit.

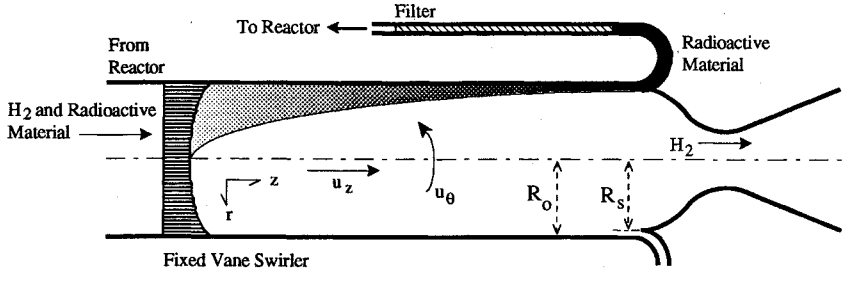

Fig. 1 Proposed swirl-based cleaning system.

The computational flow model solved the Euler equations for an axisymmetric geometry to obtain the steady-state solution for the flow in the separation chamber. The governing equations for an axisymmetric flow with swirl can be written in nonconservative form as

$$\frac{\partial \boldsymbol{U}}{\partial t} + \frac{\partial \boldsymbol{E}}{\partial z} + \frac{\partial \boldsymbol{F}}{\partial r} + \boldsymbol{G} = 0 \tag{5}$$

Where $\boldsymbol{U}, \boldsymbol{E}, \boldsymbol{F}$, and $\boldsymbol{G}$ are given by the following expressions:

$$\boldsymbol{U} = \begin{bmatrix} \rho \\ \rho u_z \\ \rho u_r \\ \rho u_\theta \\ [1/(\gamma - 1)]p + \frac{1}{2}\rho|\boldsymbol{V}|^2 \end{bmatrix} \tag{6}$$

$$\boldsymbol{E} = \begin{bmatrix} \rho u_z \\ p + \rho u_z^2 \\ \rho u_z u_r \\ \rho u_z u_\theta \\ [\gamma/(\gamma - 1)]pu_z + \frac{1}{2}\rho u_z|\boldsymbol{V}|^2 \end{bmatrix} \tag{7}$$

$$\boldsymbol{F} = \begin{bmatrix} \rho u_r \\ \rho u_z u_r \\ p + \rho u_r^2 \\ \rho u_r u_\theta \\ [\gamma/(\gamma - 1)]pu_r + \frac{1}{2}\rho u_r|\boldsymbol{V}|^2 \end{bmatrix} \tag{8}$$

$$\boldsymbol{G} = \begin{bmatrix} (\rho u_r/r) \\ (u_z u_r \rho/r) \\ -(\rho u_\theta^2/r) + (\rho u_r^2/r) \\ (2\rho u_r u_\theta/r) \\ (\{[\gamma/(\gamma - 1)]pu_r + \frac{1}{2}\rho u_r|\boldsymbol{V}|^2\}/r) \end{bmatrix} \tag{9}$$

The first entry in each matrix represents the continuity equation, the next three represent momentum equations, and the last represents the energy equation for a nonconducting ideal gas. An explicit, cell-centered version of the Jameson finite volume method was used to solve these equations.[3] When applied to Eq. (5), this method can be written as

$$U_{j,k}^{n+1} = U_{j,k}^{n} - \frac{\Delta t}{A_{j,k}}\left[\sum_{m=1}^{4}(E_m \Delta y_m - F_m \Delta x_m - D_m) + A_{j,k}G_{j,k}\right] \tag{10}$$

where the summation represents the flux through each of the four sides of the cell, and D_m represents a sum of second- and fourth-order damping terms. A detailed description of these terms is given in Ref. 3. Equation (10) was iterated in a time-accurate manner using a four-step Runge-Kutta discretization that can be written as

$$U_{j,k}^{p} = U_{j,k}^{n} - \frac{\Delta t}{(5 - p)A_{j,k}}\left[\sum (E\Delta y - F\Delta x - D) + A_{j,k}G_{j,k}\right] \tag{11}$$

$$U_{j,k}^{n+1} = U_{j,k}^{4}$$

where p is incremented from 1 to 4 during each time step.

The upper and lower boundary conditions are specified by imposing zero mass flux through the upper wall and centerline. Since the outgoing flow is supersonic, the outlet conditions can be extrapolated from the interior of the flow. The inlet conditions are more complicated and merit discussion.

The inlet flow conditions are determined by coupling conditions in the swirler and combustion chamber to downstream conditions via the J_- Riemann invariant.[4] The four conditions that are imposed from outside the system are 1) that the flow's radial velocity is zero, 2) that the flow's swirl velocity is a function of radius only, 3) that the flow's total enthalpy is everywhere equal to the total enthalpy in the combustion chamber, and 4) that the flow's entropy is given by Crocco's steady-state relation. The assumption that the inlet flow is cylindrical is also imposed through Crocco's relation. Together, these requirements can be written as

Upstream conditions

$$u_r = 0 \tag{12}$$

$$u_\theta = f(r) \tag{13}$$

$$C_p T_c = C_p T = \tfrac{1}{2}(u_z^2 + u_\theta^2) \tag{14}$$

$$\nabla H = T\nabla s + (\boldsymbol{u} \times \boldsymbol{\Omega}) \tag{15}$$

Downstream condition

$$J_- = u_z - [2/(\gamma - 1)]c = \text{const} \tag{16}$$

These conditions were implemented in the following manner: u_r, u_θ, and J_- are known from outside conditions. Given these values, u_z and T can be obtained by combining Eqs. (14) and (16). The result is

$$u_z = \frac{2J_- + \sqrt{4J_-^2 - 4\{1 + [2/(\gamma - 1)]\}\{J_-^2 - T_c[4\gamma R/(\gamma - 1)^2] + [2u_\theta^2/(\gamma - 1)]\}}}{2 + [4/(\gamma - 1)]} \tag{17}$$

$$T = [(\gamma - 1)^2/4\gamma R](u_z^2 - 2u_z J_- + J_-^2) \tag{18}$$

Crocco's relation can now be used to determine the density of the flow. For a constant enthalpy flow, Eq. (15) can be written as

$$\nabla s = -C_p\{1/[H_\infty - \tfrac{1}{2}(u_z^2 + u_\theta^2)]\}(\boldsymbol{V} \times \boldsymbol{\Omega}) \tag{19}$$

Since the flow is cylindrical, the vorticity has no radial or tangential component, and the entropy gradient can be written

$$\frac{ds}{dr} = \frac{C_p \Omega_z u_\theta}{H_\infty - \frac{1}{2}(u_z^2 + u_\theta^2)} \tag{20}$$

This integral can be evaluated numerically to give s as a function of radius. Once s has been calculated, the thermodynamic definition of entropy can be combined with the equation of state to determine the flow's pressure and density, giving the following result:

$$\rho = \{(\rho_0^\gamma/P_0)[\gamma/(\gamma - 1)](C_p T)\exp(-s/C_v)\}^{1/(\gamma-1)} \tag{21}$$

where ρ_0 and P_0 are reference values taken where $s = 0$. In these simulations, the centerline was chosen as the reference point, and the P_0 and ρ_0 were calculated by assuming that the stagnation pressure along the centerline was a constant 29 atm. This is equivalent to the assumption that as the swirl velocity increases, the chamber pressure increases to compensate for losses in the swirler. The local pressure can then

be calculated using the ideal gas law. The result is a set of four equations [Eqs. (17), (18), (20), and (21)], which fully specify the inlet boundary conditions.

The flow solutions used in this study were produced using fourth-order damping with damping coefficients from 0.02–0.04 in both the r and z directions. The final solutions conserved mass flow to within 2.5% and angular momentum flux to within 4%. The deviations in these quantities are caused by the combination of discretization error and the nonconservative formulation of the equations used in this study. Although these flowfields were considered sufficiently accurate for this study, future work would benefit from the use of a conservative formulation of the axisymmetric Euler equations.

The second part of the simulation consists of a particle tracker that simulates the release of a uniform distribution of spherical particles at the entrance to the chamber. This program tracks the particles individually to determine which are caught by the skimmer, and which pass through the nozzle. The particle tracker did not model the skimmer in detail, but instead took a series of cross sections of the separation chamber and assumed that any particles with a radial position greater than R_s were caught by the skimmer. The governing equations for spherical particles in an axisymmetric swirling flow are

$$\ddot{r} - r\dot{\theta}^2 = [(F_{dr} + F_{pr})/m] \tag{22}$$

$$r\ddot{\theta} + 2\dot{r}\dot{\theta} = (F_{d\theta}/m) \tag{23}$$

$$\ddot{z} = (F_{dz}/m) \tag{24}$$

F_{pr} is usually small and can be neglected. The drag force is calculated using the usual expression

$$F_d = \tfrac{1}{2}\rho(|V - V_p|)^2\pi a^2 C_d \tag{25}$$

where C_d is the drag coefficient for a fully immersed sphere. For $0 < Re < 2.5 \times 10^5$, the drag coefficient is given by the following formula to an accuracy of approximately 10%[5]:

$$C_d = (24/Re) + [6/(1 + \sqrt{Re})] + 0.4 \tag{26}$$

where Re is the diameter-based Reynolds number based on the differential velocity between the particle and the fluid. The viscosity of H_2 is determined using a low-order approximation for the viscosity of a pure gas. The following equation gives the viscosity in units of kg/m/s[6]:

$$\mu = 2.6693 \times 10^{-26}[(MT)^{1/2}/\overline{\Omega}^{(2,2)}] \tag{27}$$

$\overline{\Omega}^{(2,2)}$ is temperature-dependent and has been recorded for H_2 by Vanderslice et al.[7] Typical values for μ at the temperatures encountered in the simulation range from 2.5×10^{-5} to 3.8×10^{-5} kg/m/s. Overall, for particles with radii under 100 μm, this model is valid at relative velocities from 0 m/s to over 10,000 m/s, and at temperatures up to 15,000 K.

Each simulation consists of the release of 500 particles at evenly spaced distances from the centerline (i.e., the first particle is released at $r = 0$, the last one at $r = R_0$). In all simulations, particles enter the chamber with an axial velocity equal to the flow's axial velocity and with a swirl velocity of zero. In practice, particles are likely to acquire some swirl while passing through the vanes, and so the assumption that the initial swirl velocity is zero is a "worst-case" assumption.

Computational Results

The computational simulation described above was used to examine the effectiveness of two types of fixed vane swirlers over a variety of operating conditions. The two devices examined were constant-angle and solid-body-rotation swirlers. In constant angle swirlers, the swirl velocity is given by

$$u_\theta = u_z \tan \psi \tag{28}$$

This relation does not apply close to the centerline, where the swirl velocity is restricted by a no-swirl boundary condition. In solid-body rotation swirlers, the governing equation is

$$u_\theta = \omega r \tag{29}$$

where ω represents the flow's rotation rate in radian/s. All of the results discussed in this section are based on solid-body rotation results. Constant angle swirlers are discussed in the section on "alternate flow profiles."

A total of five parameters were varied during the solid body rotation swirl simulations: 1) the chamber length, 2) the particle density, 3) the particle radius, 4) skimming ratio, and 5) the flow rotation rate. The particle density was varied between that of graphite, 1800 kg/m^3, and Uranium, 18,700 kg/m^3. The other parameters were varied as follows: chamber length—0 to 1 m, particle radius—1 to 100 μm, rotation rate—0 to 8000 rad/s, and skimming ratio—0 to 0.2.

The assumption of constant total pressure along the centerline caused the axial velocity in the separation chamber to vary with rotation rate. The data is therefore expressed in terms of separation times rather than in terms of the chamber length. The separation time t_s is obtained by dividing the chamber length by the mean axial velocity of the flow. It represents the time necessary to obtain a given degree of particle-flow separation.

The solid body rotation results can be characterized by several simple relationships that simplify analysis of the overall system. Figure 2 shows a graph of the system's radius-based cleaning efficiency vs skimming ratio for a series of different separation times. It shows simulated data for 40-μm graphite particles in a flow with a rotation rate of 8000 rad/s, and each point on the graph represents a simulated data point. Figure 2 clearly shows the presence of a linear relationship between the skimming ratio and the radius-based cleaning efficiency. This relationship can be written in the following form:

$$\eta' = \eta_0' + (1 - \eta_0')s_r \tag{30}$$

The solid lines on the graph are based on this approximation. It has been found that Eq. (30) accurately represents the simulated data to within 10% under all of the conditions examined in this study. Therefore, Eq. (30) and a table of reference efficiencies provide the information necessary to calculate the efficiency of the system at any skimming ratio. It should be noted that as the reference efficiency rises, changes in the skimming ratio have less effect on the system. In the operating ranges of interest to the designer, the choice of

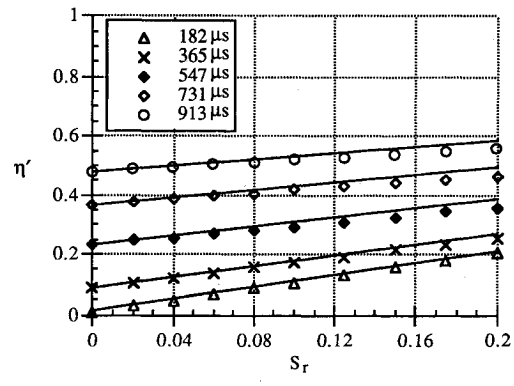

Fig. 2 Radius-based cleaning efficiency vs skimming ratio at 8000 rad/s.

skimming ratio should have relatively little effect on the cleaning efficiency. These results reflect the assumption that particles do not rebound when they collide with the wall, discussed in detail below.

The relationship of greatest interest to the designer is that between the efficiency and the flow rotation rate. We plot the efficiency vs ν, where

$$\nu = \omega t \tag{31}$$

Figure 3 shows simulated data taken at five different rotation rates, and demonstrates that data taken from a wide range of rotation rates collapse down to a single curve when plotted against ν. Using Eq. (30) and Fig. 3, a designer can determine the effectiveness of the system for any skimming ratio, rotation rate, or chamber length. Therefore, this plot contains the information necessary to carry out design studies and construct an initial design of a vortex cleaning system. Using a family of these plots, it is possible to summarize the performance of this system across a range of performance parameters. Figure 4 shows a similar plot made with a particle of different size and density. It shows that the collapse onto a single curve occurs for a variety of particle sizes and densities. The only simulated case in which this does not occur is with the 1-μm graphite particles, which are very strongly "coupled" to the flow; a condition discussed below. Figure 4 also indicates that the effectiveness of the system depends strongly on the composition of the particles in the flow. For instance, while a 1-m separation chamber operating at 8000 rad/s would remove almost 98% of the 1-μm uranium particles, it would remove at most 50% of the 20-μm uranium particles and becomes even less efficient with larger uranium particles.

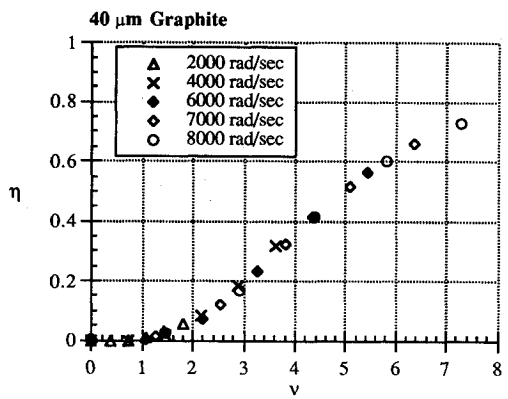

Fig. 3 Cleaning efficiency vs dimensionless frequency for solid body rotation swirlers.

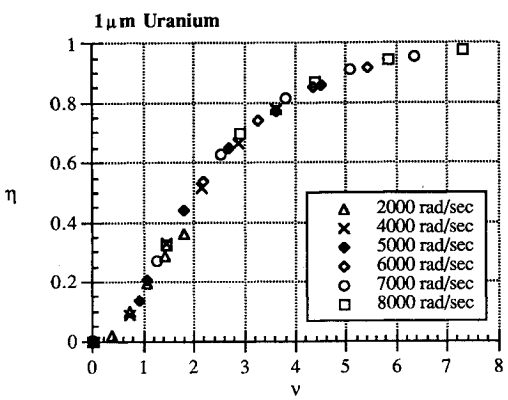

Fig. 4 Cleaning efficiency vs dimensionless frequency for solid body rotation swirlers.

Analytical Model and Fundamental Physics

One way to develop an understanding of the relationship between cleaning efficiency and particle size and composition is to construct a simple analytical model of the vortex separation process. In general, the presence of drag makes it impossible to solve the particle equations of motions using analytic methods. However, if it is assumed that particles entering the channel move at the same axial and tangential velocity as the fluid, the centrifugal forces on the particle are much larger than the forces due to particle-fluid interaction. Particles traveling in this regime are said to be "uncoupled" from the flow. This is in contrast to a particle whose motion is dominated by fluid interaction forces which is said to be coupled to the flow. Neglecting fluid forces reduces Eqs. (22–24) to the following form:

$$\ddot{r} - r\dot{\theta}^2 = 0 \tag{32}$$

$$r\ddot{\theta} + 2\dot{r}\dot{\theta} = 0 \tag{33}$$

$$\ddot{z} = 0 \tag{34}$$

Solving Eqs. (32) and (33) analytically results in the following solution:

$$t_s = (r/\omega)\sqrt{(1/r_0)^2 - (1/r)^2} \tag{35}$$

where r_0 is the particle's initial radial position. Setting $r = R_s$ gives an expression for the time it takes for a particle to move from r_0 to a position where it can be caught by the skimmer. t_s then represents the particle separation time.

Equation (35) can also be written in terms of the design parameters η' and s_r

$$\eta' = [(1 - s_r)/\sqrt{(\nu^2 + 1)}] \tag{36}$$

Equation (36) shows that there are two fundamental parameters that determine the system's efficiency: 1) the skimming ratio and 2) ν. For a given value of ν, s_r and η' are linearly related with the efficiency ratio approaching unity as s_r approaches unity. This matches the behavior seen in the simulations, particularly in Eq. (30) above. The relationship between ν and η' is less clear, because the shape of Eq. (36) does not match the curve shown in Fig. 3. It is true that in both cases, the cleaning efficiency is a function of ν. This implies that under some conditions, particles in the full simulation act as though they are uncoupled from the flow. However, since particles in the full simulation enter the chamber with a tangential velocity of zero, it is also clear that drag forces must play an important role in determining their motion.

The critical parameter that determines whether a particle is coupled or uncoupled from the flow is the ratio of the fluid-particle interaction forces to the inertial forces acting on it. The magnitude of the centrifugal forces on a particle is given by

$$F_c = (mu_{p\theta}^2/r) = (\tfrac{4}{3}\pi a^2 \rho_p u_{p\theta}^2/r) \tag{37}$$

Using this and expression (25), it can be shown that the ratio of the centrifugal to drag forces on a particle is approximately

$$\frac{F_c}{F_d} = \frac{2}{3}\frac{1}{C_d}\frac{a}{r}\frac{\rho_p}{\rho_f}\frac{u_{p\theta}^2}{(r\omega - u_{p\theta})^2} \tag{38}$$

When $u_{p\theta} = 0$, $F_c/F_d = 0$, so that the particle is strongly coupled to the fluid. As $u_{p\theta}$ approaches $r\omega$, F_c/F_d approaches infinity, and the particle is uncoupled from the fluid. In-between these extremes, there is a critical coupling velocity v_c, where $F_c/F_d = 1$. When $u_{p\theta}$ is much less than v_c, a particle is coupled to the flow, and when $u_{p\theta}$ is much greater than v_c, it

is uncoupled from the flow. A particle entering with a tangential velocity of zero is initially coupled to the fluid, but eventually uncouples as it experiences tangential acceleration.

Figure 5 shows the approximate value of the force ratio F_c/F_d vs $u_{p\theta}$ for graphite and uranium particles under conditions similar to those used in the computer simulations. Each particle's coupling velocity is indicated by the point at which the curve crosses the solid line. As one would expect, Fig. 5 shows that F_c/F_d is zero when $u_{p\theta} = 0$, and approaches infinity as u_θ approaches $r\Omega$. Figure 5 also shows that small particles with low densities have very high coupling velocities. At intermediate velocities, the relative importance of F_c and F_d depends on the size and density of the particle being analyzed. Comparing the simulated data with Fig. 5 showed that particles with coupling velocities in an intermediate range (between 200–800 m/s) have relatively high recovery rates, while those at the high and low end of the range have relatively low recovery rates. The reasons for this correlation are evident in Fig. 6, which shows that particles with different coupling velocities follow radically different paths in the separation chamber.

All three of the particles shown in Fig. 6 begin at the same location. The 1-μm graphite particle, which has a high coupling velocity, follows a long spiral path towards the outside wall. The 100-μm particle, which has a low coupling velocity, travels directly down the channel and ignores the influence of the fluid altogether. Neither particle is moved to the outside of the flow in a particularly efficient manner. In the first case, although the particle is quickly accelerated to a high tangential velocity, drag forces dominate its motion and prevent it from gaining radial velocity. In the second case, the particle's motion is dominated by inertial forces, and so it never gains tangential velocity. The particles that are separated most efficiently are those with intermediate coupling velocities. These particles remain coupled to the fluid long enough to reach a high tangential velocity, and then uncouple as they travel towards the outside of the channel.

Equation (38), then, defines another parameter that is of importance to the designer. The critical coupling velocity determines the effectiveness of the vortex separation system and determines which types of particles can and cannot be removed by a given separation geometry. Given specific data on the distribution of particles in a nuclear rocket plume, Eq. (38) can be used to determine what portion of the radioactive material will be removed efficiently from the flow. At the present time, however, such data is not available, and all that can be said with certainty is that vortex separation systems will be most effective on particles with coupling velocities in an intermediate range.

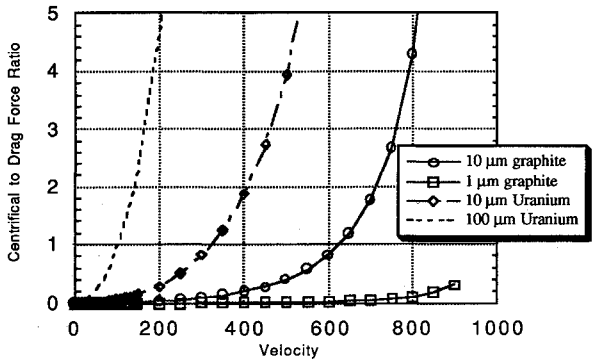

Fig. 5 Ratio of centrifugal to drag force as a function of tangential velocity.

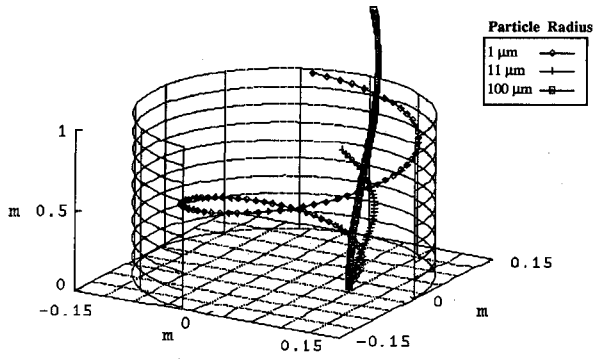

Fig. 6 Particle tracking data.

Alternative Flow Profiles and Results

Although solid body rotation swirlers are convenient to characterize and study, they distribute swirl energy in a relatively inefficient manner. In particular, because they create higher swirl velocities at the outside of the flow, they tend to give the greatest acceleration to those particles that are closest to the edge of the chamber. Constant angle swirlers distribute energy more evenly across the flow, and are therefore better suited to particle removal. To simulate constant angle swirlers, a series of simulations was conducted using the swirl profile defined in Eq. (28), but with the velocity tapering off linearly from zero at the centerline to its proper value at $0.2R_0$. This core of solid body rotation is necessary to meet the centerline no-swirl condition. The profiles studied correspond to turning angles ranging from 0 to 35 deg.

Figure 7 shows a plot of constant angle rotation data for 40-μm graphite particles at a turning angle of 35 deg. Data is presented in a plot of radius-based cleaning efficiency vs skimming ratio and separation time. The solid lines indicate curve fits made using Eq. (30). A comparison of this plot to the equivalent data in Fig. 2 shows that the efficiencies in this case are quite a bit higher than those in Fig. 2, even though the maximum flow turning angle represented in Fig. 2 is approximately 50 deg (the value at the outer radius when the rotation rate is 8000 rad/s). Figure 7 also shows that Eq. (30) no longer fits the simulated data, and so a table of reference values is no longer sufficient to calculate the cleaning efficiency at an arbitrary skimming ratio. To fully characterize this system, it is necessary to collect data at each individual skimming ratio. Figure 8 shows two graphs of simulated constant angle efficiency data vs a dimensionless frequency based on the rotation rate in the core solid body rotation region. Although the values of ν differ, this data was taken over a range of conditions similar to that covered in Figs. 3 and 4.

Figure 8 shows that the constant angle swirlers are considerably more effective than their solid body rotation counterparts. Under some conditions, constant angle swirlers can easily remove 99% of the material in the flow, even at moderate turning angles. In addition, constant angle swirlers are able to remove a wider distribution of material from the flow than their solid body rotation equivalents. With a 1-m-long

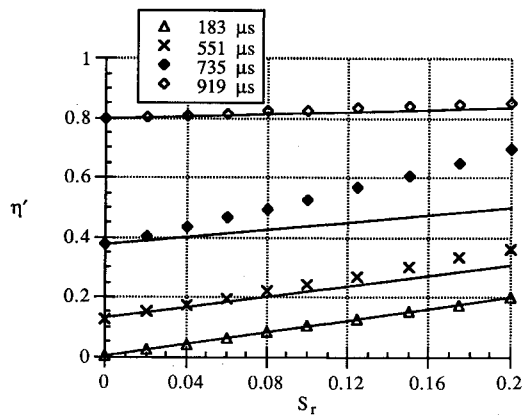

Fig. 7 Radius-based skimming efficiency vs skimming ratio at the turning angle of 35 deg.

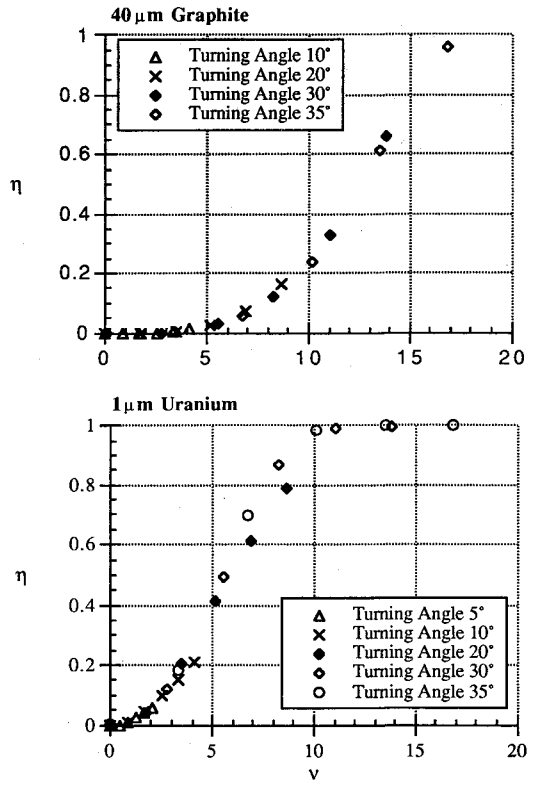

Fig. 8 Efficiency data for constant angle swirlers.

Table 1 Efficiency vs skimming ratio with elastic collisions

Skimming ratio	Cleaning efficiency
0.020	0.425
0.040	0.625
0.060	0.734
0.080	0.842
0.100	0.920
0.125	0.956
0.150	0.976
0.175	0.992
0.200	0.995

Chamber length = 1 m.

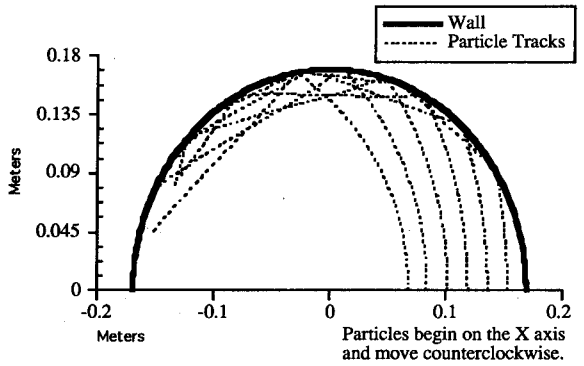

Fig. 9 Paths of particles including elastic wall-particle collisions.

separation chamber and a skimming ratio of 0.1, the simulated constant angle system can remove more than 90% of all the graphite particles in the flow with radii from 10–50 μm. Therefore, a practical cleaning system would probably be designed around a constant angle swirl profile or something similar to it. Given further work, it may be possible to develop more effective flow profiles that will distribute swirl energy more efficiently across the flow and enhance the system's efficiency over a wide distribution of particle sizes and densities.

Particle-Wall Interaction Effects

The results presented to this point are based on the assumption that particles that strike the walls of the separation chamber are trapped in the boundary layer and eventually enter the skimmer. This implies that the wall has a restitution coefficient of zero. In reality, particles impacting the wall may bounce and re-enter the main flow. If the particle has a low enough coupling velocity, it will act as though the flow is not present, and particle-wall collisions will dominate its motion.[8] The particles of interest in this study, however, are those with intermediate coupling velocities. To examine the effect of particle-wall collisions on these particles, several simulations were conducted in which particles that struck the wall were assumed to undergo fully elastic collisions (i.e., the normal velocity component was reversed while the tangential velocity component remained constant). Figure 9 shows typical particle trajectories for 40-μm graphite particles traveling in a 35-deg constant angle flow projected onto the r-θ plane.

Figure 9 shows that when particles with intermediate coupling velocities strike the wall, they are confined to a relatively narrow region along the outside of the separation chamber. This occurs because the particles still have a considerable tangential velocity after each collision that quickly returns them to the outside wall. Based on this observation, one can make several general comments about the effects of inelastic collisions on the particles. Wall-particle collisions that cause the particle to lose normal momentum without losing tangential momentum will lower the width of the confinement region, while collisions that cause the particle to lose tangential momentum without losing normal momentum will widen this region. Determining exactly how a particle would react to a series of inelastic collisions requires detailed knowledge of the particle's angular momentum as well as the shape and composition of the wall, and is therefore left for future work.

It should be noted that the width of the confinement region sets a practical lower limit on the skimming ratio. The results presented in Fig. 8 give a nominal efficiency of 99.0% for 40-μm graphite particles at a skimming ratio of zero. The fully elastic collision model gives different results that are summarized in Table 1.

Table 1 shows that elastic wall-particle collisions have a large influence on the cleaning efficiency when the skimming ratio is small, but have very little effect once the skimming ratio exceeds 0.15. Based on this observation, it can be said that the results present in Figs. 3–9 are valid above a certain limiting value of the skimming ratio. The exact value of this limit depends on the size and composition of the particles in the flow, and will be very high for particles with low coupling velocities. A designer's choice of skimming ratio depends not only on the desired efficiency, but also on thrust loss considerations. This point is discussed below in more detail.

Limits on System Efficiency

The results presented to this point show that it is desirable to make the swirl number as high as possible, as higher swirl rates lead to lower separation times and, thus, to shorter separation chambers. There are, however, practical limits to the amount of swirl that can be imparted to the flow without causing performance losses. An absolute limit is set by the need to avoid vortex breakdown. Vortex breakdown refers to a phenomenon in which the structure of the swirling flow is suddenly destroyed by a spontaneous and pronounced retardation of the flow and a divergence of stream surfaces near the core of the vortex.[9] If breakdown were to occur in the separation chamber, it would destroy the structure of the flow and cause a large drop in flow velocity. Breakdown is gen-

erally found in highly swirling flows and in the presence of adverse pressure gradients, although boundary-layer effects can produce breakdown in parallel geometries like the one proposed for the separation chamber. Although the mechanism by which breakdown occurs is poorly understood, experimental data indicates that the possibility of vortex breakdown exists in situations where the flow turning angle is greater than 40 deg.[9] Therefore, in the geometry tested, the threat of vortex breakdown precludes the use of solid body rotation rates greater than 6000 rad/s and of constant angle turning rates greater than 40 deg.

Another issue of concern is the effect of swirl on the thrust and specific impulse of the rocket. The available experimental data indicates that the addition of constant angle swirl to the flow has virtually no effect on the specific impulse, even when the swirl angle reaches 40–45 deg.[10] The thrust of the engine is affected, however, as the addition of swirl results in lower mass flow through the throat. The available data indicates that the addition of 40–45-deg constant angle swirl to the flow results in a thrust loss of about 5%.[10] It may, however, be possible to compensate for swirl thrust losses by raising the chamber pressure and, thus, compensating for stagnation pressure losses induced by the swirler.

Additional thrust losses would be induced by the skimmer. These losses are proportional to the mass flow removed from the core of the flow and are, therefore, strongly related to the skimming ratio. A lower limit to the skimming ratio is set by the need to capture particles after they collide with the walls of the separation chamber. The exact value necessary depends on the nature of the particle wall interaction. In the case described in Table 1, a skimming ratio of at least 0.1 is clearly desirable. For small values of s_r, the fraction of the mass flow removed is approximately twice the skimming ratio. This means that a skimming ratio of 0.1 (a 1.6-cm slot for the geometry shown in Fig. 1) would cause a thrust loss of 20%. Therefore, a practical vortex separation system could end up causing very significant thrust losses. The actual thrust loss would depend on details of the particle-wall interactions and the desired removal efficiency.

There is also a question of whether it is possible to build a fixed angle swirler that can withstand a 2500 K flow. The high temperature, combined with the high density and specific heat of the hydrogen in the flow, will produce severe heating problems in the swirler. Although experimental jet engines have operated with turbine temperatures in the range of 2300–2500 K,[11] these operating temperatures are clearly at the state-of-the-art. In addition, the high specific heat of hydrogen would probably increase the heat transfer to the blade, although this effect might be mitigated by the use of hydrogen as a working fluid for active cooling of the blade. These cooling issues place serious constraints on the effectiveness of the system and further work is required on the design of the swirler and its cooling system if this separation scheme is to be implemented in a practical manner.

Finally, it should be noted that the results presented in this article are based on the assumption of laminar flow in the separation chamber. A turbulent flow description could substantially alter the results presented above, particularly for particles with high coupling velocities. Further theoretical work is needed to clarify the influence of turbulence on the system's cleaning efficiency.

Conclusions

This article contains a detailed analysis of a vortex cleaning system designed to remove radioactive material from the plumes of nuclear rockets. A computational analysis of this system indicates that it can operate with particle removal efficiencies in excess of 99%, but that its effectiveness depends heavily on the sizes and densities of the particles in the flow. Due to a lack of experimental data, it is impossible to state whether or not this system is suitable for use on real nuclear rockets. However, this article does identify v_c as the parameter that determines the effectiveness with which the system removes a particle of given size and density. Once the size and composition of the particles in a nuclear rocket plume have been determined, it will be possible to calculate their critical coupling velocities and determine the potential effectiveness of a swirl-based particle cleaning system.

This article also identifies a dimensionless frequency as a parameter of interest to the designer. The dimensionless frequency determines the relationship between the flow rotation rate and the length of the separation chamber. The performance of both constant angle and solid body rotation systems is governed by the coupling velocity and the dimensionless frequency parameters. In addition, there is one other parameter, the skimming ratio, which has relatively little influence on the cleaning efficiency, but does determine the thrust/mass losses associated with this system. A lower limit on the skimming ratio is set by wall-particle interaction effects. Above this limit, the efficiency should be equivalent to that calculated under the assumption that all particles that strike the wall are captured by the skimmer. Using these three parameters, it should be possible to conduct basic design studies on this swirl-based cleaning system.

In conclusion, the vortex separation system proposed in this article shows some promise. By customizing the swirl profile, it should be possible to remove most of the particles in the plume before they leave the nozzle. There should, however, be substantial mass and thrust penalties associated with this system, particularly if it is necessary to remove particles with nonintermediate coupling velocities. Further experimental work is required to verify these computational results and to determine the size and composition of the radioactive material in actual nuclear rocket plumes. Once such data is available, this article identifies the parameters that are of interest to the designer, and provides the tools necessary to estimate the effectiveness of the system based on those parameters.

Acknowledgments

This work was funded by the Air Force Office of Scientific Research, Bolling AFB, Washington, DC, Grant AFOSR-91-0415.

References

[1]Kirk, W. L., "Nuclear Furnace-1 Test Report," N-Div. and CNC-Div., Los Alamos Scientific Lab., LA-5189-MS, Los Alamos, NM, March 1973.

[2]Traineau, J. C., Kuentzmann, P., Prévost, M., Tarrin, P., and Delfour, A., "Particle Size Distribution Measurements in a Subscale Motor for the Ariane 5 Solid Rocket Booster," AIAA Paper 92-3049, July 1992.

[3]Jameson, A., Schmidt, W., and Turkel, E., "Numerical Solutions of the Euler Equations by Finite Volume Methods Using Runge-Kutta Time-Stepping Schemes," AIAA Paper 81-1259, June 1981.

[4]Hirsch, C., *Numerical Computation of Internal and External Flows*, Vol. 2, Wiley, Chichester, England, UK, 1990, pp. 162–165.

[5]White, F., *Viscous Fluid Flow*, McGraw-Hill, New York, 1974, p. 209.

[6]Hirschfelder, J. O., Curtiss, C. F., and Bird, R. B., *Molecular Theory of Gases and Liquids*, Wiley, New York, 1954.

[7]Vanderslice, J. T., Weissman, S., Mason, E. A., and Fallon, R. J., "High-Temperature Transport Properties of Dissociating Hydrogen," *Physics of Fluid*, Vol. 5, No. 2, 1962, pp. 155–164.

[8]De Jong, F., Sabnis, J., and McConnaughey, P., "A Combined Eulerian-Lagrangian Two-Phase Flow Analysis of SSME HPOTP Nozzle Plug Trajectories: Part I-Methodology," AIAA Paper 89-2347, July 1989.

[9]Hall, M. G., "Vortex Breakdown," *Annual Review of Fluid Mechanics*, Vol. 4, Annual Reviews, Palo Alto, CA, 1972, pp. 195–229.

[10]Dutton, J. C., "Swirling Supersonic Nozzle Flow," *Journal of Propulsion and Power*, Vol. 3, No. 4, 1987, pp. 342–349.

[11]Kerrebrock, J. L., *Aircraft Engines and Jet Turbines*, 2nd ed., MIT Press, Cambridge, MA, 1992, p. 296.